Segregation of Granular Particles by Mass, Radius, and Density in a Horizontal Rotating Drum

M. M. H. D. Arntz
Food Process Engineering Group, Wageningen University, 6700 EV Wageningen, The Netherlands

H. H. Beeftink
Bioprocess Engineering, Wageningen University, 6700 EV Wageningen, The Netherlands

W. K. den Otter
Computational Biophysics and MESA+ Institute for Nanotechnology, University of Twente, 7500 AE Enschede, The Netherlands

Multiscale Mechanics and MESA+ Institute for Nanotechnology, University of Twente, 7500 AE Enschede, The Netherlands

W. J. Briels
Computational Biophysics and MESA+ Institute for Nanotechnology, University of Twente, 7500 AE Enschede, The Netherlands

R. M. Boom
Food Process Engineering Group, Wageningen University, 6700 EV Wageningen, The Netherlands

DOI 10.1002/aic.14241
Published online October 1, 2013 in Wiley Online Library (wileyonlinelibrary.com)

The impact of particle properties on segregation and mixing of bidisperse granular beds in a rotating horizontal drum have been studied by discrete element method (DEM) simulations. Bidispersities in radius, density, and mass have pronounced influences on the stationary mixing pattern, although they hardly affect the granules' flow regime. At 50% fill level, all beds mix well for a Froude number of ~0.56, corresponding to a flow regime intermediate to cascading and cataracting, while segregation occurs both at lower (rolling and cascading regime) and higher (cataracting/centrifuging regime) Froude numbers. These observations are explained qualitatively by noticing that the angular drum velocity dictates the flow regime, which in turn determines the effectiveness and direction of four competing (de)mixing mechanisms: random collisions, buoyancy, percolation, and inertia. A further dozen particle properties have been varied, including the friction coefficients and elastic modulus, but these proved inconsequential to the steady-state degree of mixing. © 2013 American Institute of Chemical Engineers *AIChE J*, 60: 50–59, 2014
Keywords: discrete element simulation, particle mixing, bidisperse, Froude, angular velocity

Introduction

Mixing of granular solids in a rotating horizontal drum is a routine processing step in a wide range of industries. Notwithstanding the numerous practical applications, the understanding of granular materials is still incomplete.[1,2] The flow and (de)mixing behavior of granular beds have turned out to be surprisingly complex phenomena—a change in the operational conditions or in the granular particles' properties can readily result in a sub-optimal mixing process, or even cause demixing of the particles, with obvious consequences for the product quality.[3–5] The practical importance and intriguing complexity have made granular mixing the subject of intense research in the last decades, as summarized in various reviews,[6–10] but the translation of the more fundamental findings into reliable predictions for practical processes is still incomplete.[2,11,12]

Bidisperse granular beds of industrial relevance usually contain particles that differ in size and/or specific gravity, hence the separate and combined effects of these two granular properties on the (de)mixing process are central in this paper. The mixing and segregation behavior of granules bidisperse in size has been studied extensively, with a strong emphasis on half-filled beds in the rolling regime.[1,3,4,13–17] For slowly rotating drums it is well established that the smaller particles tend to aggregate within the first few revolutions into a radial core, surrounded by a periphery of larger particles, stretching along the entire length of the drum. This segregation process is attributed to dynamic sieving, that is the smaller particles falling through the temporary voids between the larger particles.[18] Radial streaks occur for size ratios below ~1/2.[19,20] Other studies have focused on equally sized granules bidisperse in density,[21–23] showing that the denser (and hence heavier) particles locate near the

Correspondence concerning this article should be addressed to H. H. Beeftink at rik.beeftink@wur.nl.

central axis of the bed. This segregation is generally attributed to buoyancy. Studies with simultaneous variations in both granular size and density,[12,19,24,25] again with an emphasis on half-filled beds in the rolling regime, indicate that the combination of percolation and buoyancy may enhance as well as reduce segregation. In long drums, the initial radial segregation is followed by a slow axial segregation, giving rise to stripes perpendicular to the drum's axis that gradually diffuse and merge over time.[26–30] The role of the drum's end-walls in initiating this transition, especially in narrow drums, has recently attracted attention.[31–34] Interestingly, the power consumption of a drum rotating at constant angular velocity was recently observed to correlate with the order of the granular bed in that drum.[31] Despite the extensive research and industrial relevance of segregation in tumbling blenders, to quote a recent paper:[34] "its mechanisms are not clearly understood and all known theories or explanations have exceptions." In this context, it is interesting to note that certain systems appear not to converge to a steady state, but to alternate randomly between two metastable states.[35]

While most studies on mixing and radial segregation have focused on the rolling regime, the behavior of bidisperse beds at higher drum angular velocities has received relatively little attention, especially in simulation studies.[36,37] In this paper, we report a simulation study on the interplay between size, mass, and density during mixing and segregation processes in half-filled drums in the rolling, cascading, cataracting, and cataracting-centrifuging regimes (following the definitions of flow regimes by Henein et al.[38] and Mellmann[39]). With increasing drum angular velocity, the degree of mixing is observed to initially increase, go through a maximum in between the cascading and cataracting regimes, and finally decrease again. These observations agree with experimental data.[40] Interestingly, within the sampled parameter space, all simulated systems mix very well at the same angular velocity, corresponding to a Froude number of $\sim$0.56. We will also briefly comment on the influence of other particle properties, notably the friction coefficients, compressibility and restitution coefficient, but their effects on the mixing and segregation behavior of the bed turn out to be of minor importance.

Our chosen research approach is the Discrete Element Method (DEM), that is numerical simulations of the three-dimensional translational and rotational motions of all particles in the bed, because it offers unparalleled control over the properties of the particles.[10,41,42] Simulations also provide detailed information in abundance, for example on the paths followed by individual particles or the local velocity difference between particles of distinct types. But this wealth of data does not always provide conclusive information on why the particles move the way they do. Hence, in addition to deducing the dominant segregation mechanism(s) for a given set of particle properties from the analysis of individual simulations, we will also exploit clues obtained by comparing simulations with distinct particle properties.

The structure of this paper is as follows: in the following two sections we first describe the four segregation and mixing mechanisms at work in a rotating drum, followed by details on the simulation model and the method employed to quantify the degree of mixing. Next, the simulation results are described and discussed in terms of the four segregation and mixing mechanisms. We end with a summary of the main conclusions.

Background

The mixing and segregation of bidisperse particles in granular beds is the cumulative effect of a number of mechanisms. In this paper, we will distinguish four mechanisms—random collisions, buoyancy, percolation, and inertia—with the objective of attributing, whenever possible, the observed bed behavior to a specific mechanism or a combination of mechanisms. As the definitions of these mechanisms vary across the literature,[12,14,24,43,44] we first briefly discuss our interpretations. The numerous random collisions between granules in the flowing layer promote mixing of the particles. A difference in particle specific densities (i.e., particle mass divided by particle volume) gives rise to buoyancy, causing less-dense particles to rise up and denser particles to sink down in a mobile bed. While random collisions and buoyancy are the two mechanisms that would feature in a statistical mechanical description, as the sources of maximum entropy and minimum energy, respectively, such a description is known to fail for granular systems[2,45] and two additional mechanisms have to be considered. Percolation, also known as dynamic sieving, is the ability of particles to pass through temporary cavities in porous regions of a bed; as small pores are more abundant than large pores, this mechanism will separate particles by size. The final mechanism is inertia, the resistance of any stationary or moving object to a change in its state of motion; a collision between two unequal particles will deflect the light particle more from its initial trajectory than the heavy particle and thereby promote mixing of the lighter particles, especially for the freely flying granules at Froude numbers close to one. Inertia also gives rise to centrifugal pseudo forces at high angular drum velocities, which alter the direction of the buoyancy and percolation mechanisms: the denser or smaller particles, respectively, are now moving radially outward rather than vertically down. Note that the particle's mass, radius, and density are not mutually independent, which in practice readily obfuscates the distinction between the segregation mechanisms. As the determination of the dominant segregation mechanism(s) from a single simulation is often not clear-cut, we obtain additional insights into the segregation mechanism by analyzing the changes that occur—or do not occur—upon varying specific particle properties. The granular mixtures investigated here have been chosen with the aim of highlighting or suppressing certain segregation mechanisms, in order to elucidate their roles. An improved appreciation of these four mechanisms, whose relative contributions vary across the various flow regimes, allows more accurate predictions of the steady-state degree of mixing or segregation in practical situations.

Model Description and Characterization of Mixing

The DEM simulates the translational and rotational dynamics of spherical granules by numerically integrating their equations of motion.[43,45–48] The normal force exerted on particle i by particle j is described by a linear spring and dashpot model

$$\mathbf{F}_{ij}^{n} = -k_{pp}^{n}\delta_{ij}\hat{\mathbf{n}}_{ij} - \eta_{ij}^{n}\mathbf{v}_{ij}^{n} \tag{1}$$

with k_{pp}^{n} the elastic stiffness of the particles, δ_{ij} their apparent overlap distance, $\hat{\mathbf{n}}_{ij}$ the normal unit vector from the center of particle i to the center of particle j, η_{ij}^{n} the normal damping coefficient, and $\mathbf{v}_{ij}^{n} = \left(\mathbf{v}_i - \mathbf{v}_j\right) \cdot \hat{\mathbf{n}}_{ij}\hat{\mathbf{n}}_{ij}$ their relative

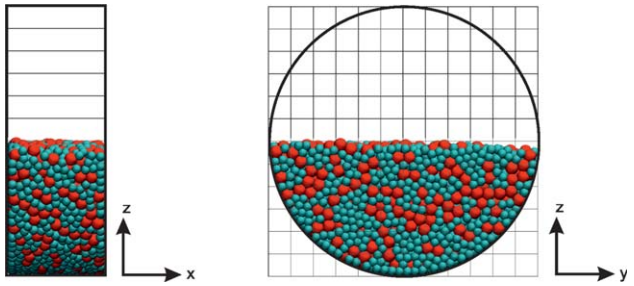

Figure 1. Front view (left) and side view (right) illustrating the relative dimensions of the drum and the two particle radii.

The fill level is 50% in all simulations. The grid of thin lines mark the cell dimensions used in the calculation of the order parameter. [Color figure can be viewed in the online issue, which is available at wileyonlinelibrary.com.]

velocity along this normal. The Coulomb model of tangential friction distinguishes between sticking and sliding regimes. In Schäfer's approximation[49] of the sticking regime, two touching particles are sliding very slowly with a tangential force

$$\mathbf{F}_{ij}^{t} = -\eta_{pp}^{t}\mathbf{v}_{ij}^{t} \tag{2}$$

where η_{pp}^{t} denotes the tangential or shear damping coefficient and the tangential velocity difference at the point of contact is given by $\mathbf{v}_{ij}^{t} = (\mathbf{v}_i - \mathbf{v}_j) - \mathbf{v}_{ij}^{n} + (r_i\boldsymbol{\omega}_i + r_j\boldsymbol{\omega}_j)\times\hat{\mathbf{n}}_{ij}$, with r_i the radius and ω_i the angular velocity of particle i. The friction force in the sliding regime, which doubles as the maximum attainable friction force in the sticking regime, reads as

$$\mathbf{F}_{ij}^{t} = -\mu_{pp}^{t}|\mathbf{F}_{ij}^{n}|\hat{\mathbf{t}}_{ij} \tag{3}$$

with μ_{pp}^{t} the dynamic friction coefficient and $\hat{\mathbf{t}}_{ij}$ the unit vector along the tangential velocity difference. The interactions of particles with the drum walls are of the same structure as the particle–particle interactions, where the overlap distances, normal vectors, and velocity differences are now calculated relative to the contact point(s) with the walls, and where the mechanical parameters are replaced by k_{pw}^{n}, η_{pw}^{n}, and μ_{pw}^{t}. The cylindrical drum wall of radius R and length L is oriented with its rotation axis along the y-axis and is closed by flat walls at both ends, see Figure 1. The particles also experience a gravitational pull $F_i^g = m_i g$ in the negative z-direction, with m_i the mass of the particle and $g = 9.8$ m/s^2 the standard gravitational acceleration. We solve the particles's motions by numerically integrating Newton's second law of motion, for the preceding forces and their corresponding torques, using the Verlet "leap-frog" scheme[50] with a fixed time step $\Delta t = 2\times10^{-6}$ s. This small step was chosen to obey energy conservation in elastic particle–particle and particle–wall collisions (i.e., at zero friction) and to obey momentum and angular momentum conservation in elastic and inelastic collisions. We also verified for selected runs that in the stationary state the average rate of energy insertion into the bed by the rotating drum walls is in agreement with the power dissipated in the bed by the various friction forces.[31]

The simulation parameters of our reference system are listed in Table 1, together with the ranges of parameter variations employed in this study. For comparison purposes, this reference system is identical to that in our prior study

Table 1. Simulation Parameters of the Granules and the Drum

Parameter (unit)	Reference	Range
Radius r_a of a particle (mm)	1	–
Radius r_b of b particle (mm)	1.5	1.0 or 1.5
Volume fraction a and b particles	1	–
Number fraction a and b particles	$3\frac{3}{8}$	1 or $3\frac{3}{8}$
Particle specific gravity (kg/m^3)	2500	2500–9191
Particle–particle restitution coefficient[a] e_{pp}^{n}	0.831	0–1
Particle–wall restitution coefficient[a] e_{pw}^{n}	0.9	0–1
Particle–particle dynamic friction coefficient μ_{pp}^{t}	0.5	0.05–3.5
Particle–wall dynamic friction coefficient μ_{pw}^{t}	1.5	0.015–5
Particle–particle static friction coefficient η_{pp}^{t} (kg/s)	1	0.001–2
Particle–wall static friction coefficient η_{pp}^{t} (kg/s)	3	0.003–5
Elastic stiffness coefficients k_{pp}^{n}, k_{pw}^{n} (N/m)	125	125–5000
Fill level	50%	–
Drum length L (mm)	25	–
Drum radius R (mm)	35	–
Drum angular velocity Ω (rad/s)	–	1.57–19
Froude number	–	$9\cdot10^{-3}$–1.3
Simulation time step (s)	$2\cdot10^{-6}$	–
Run length (revolutions)	30	–

Various particle properties were varied, over the ranges indicated in the third column, to assess their influence on the segregation and mixing behavior of the rotating bed. The reference system is equivalent to System 1 in Table 2.
[a]The restitution coefficients e_{pp}^{n} and e_{pw}^{n} measure the fraction of energy conserved in head-on rotation-less particle-particle and particle–wall collisions, respectively, and are functions of the mass, the elasticity coefficient k_{pp}^{n} or k_{pw}^{n}, and normal damping coefficients η_{ij}^{n} or η_{wi}^{n} of the involved particle(s).[1]

on the influence of the drum operational conditions on the mixing behavior.[48] As will be discussed in detail in the section Results and Discussion, of all varied particle properties the three most important ones turn out to be the radius, mass, and density. To assess their impact, we have studied the six bidisperse systems listed in Table 2, which includes the reference system as System 1. Three of these combinations were selected to eliminate a particular segregation mechanism; equal densities in System 1, equal radii in System 2, and equal masses in System 5. The other combinations were chosen to study the cooperation or opposition of two segregation mechanisms.

The homogeneously mixed starting configurations of the simulations were created by placing particles randomly in the entire volume of the drum, whilst avoiding overlap, followed by a short simulation to compact the bed under the influence of gravity. After all particles had settled, their velocities were zeroed before setting the drum in motion. A similar procedure was followed for block-wise segregated starting configurations, the only difference being that the

Table 2. Overview of Six Bidisperse Granular Beds

System	r_a (mm)	r_b (mm)	ρ_a (kg/m^3)	ρ_b (kg/m^3)	m_a (mg)	m_b (mg)
1	1.0	1.5	2500	2500	10.5	35.3
2	1.0	1.0	7500	2500	31.4	10.5
3	1.0	1.5	2500	7500	10.5	106.
4	1.0	1.5	7500	2500	31.4	35.3
5	1.0	1.5	7500	2220	31.4	31.4
6	1.0	1.5	9191	2220	38.5	31.4

Particles of type a accumulate in the center of the bed at low angular velocities and against the drum wall at high angular velocities. System 1 is the reference system described in Table 1.

particles of one type were randomly placed in the semicylindrical volume in front of the drum axis ($y > 0$) and the particles of the other type in the remaining semicylindrical volume behind the drum axis ($y < 0$). The number of particles in the drum was either 4420 or 6820, depending on the size of the smallest particle (see Table 2), and always corresponded to a fill level of approximately 50%.

Several methods have been developed to quantify the degree of mixing or segregation of a granular bed[11–13,51–54]. Here, we will employ a method based on the usual mixing entropy of statistical mechanics

$$S(t) = \sum_{k \in \{a,b\}} \int \rho(\mathbf{r}) x_k(\mathbf{r}) \ln x_k(\mathbf{r}) d\mathbf{r} \tag{4}$$

with $\rho(\mathbf{r})$ the local number density, $x_k(\mathbf{r})$ the local fraction of k-type particles at position $\mathbf{r}$ in the drum, and t denoting time. In practice, this integral is calculated by using a $12 \times 1 \times 12$ grid of rectangular cells, see Figure 1. A subsequent normalization relative to the mixing entropies S_{mix} of a perfectly mixed and S_{seg} of a perfectly segregated system

$$\varphi(t) = \left(S(t) - S_{\text{seg}}\right) / \left(S_{\text{mix}} - S_{\text{seg}}\right) \tag{5}$$

results in a conveniently scaled mixing parameter running from $\phi = 0$ for a fully segregated system to $\phi = 1$ for a homogeneously mixed system. Based on visual inspection of snapshots and movies, created from the regularly stored configurations by the visual molecular dynamics (VMD) package,[55] we qualify a system as "mixed" for $\phi \geq 0.9$ and as "segregated" for $\phi \leq 0.65$. A more detailed explanation of this mixing parameter is given elsewhere.[48] The simulations typically lasted for 30 revolutions to ensure that a steady state had been reached, while several simulations, especially those deep in the centrifuging regime, required longer runs. For initially homogeneously mixed beds, the mixing parameter typically steadily decays from the start value $\phi = 1$ to its final value, while initially block-wise segregated beds often pass through a mixed intermediate state before (partly) demixing again to reach their final state.[48,56]

Results and Discussion

DEM simulations were performed over a wide range of angular drum velocities Ω for all six particle mixtures of Table 2. The flow profiles of the granular beds at a discrete set of angular velocities were characterized, by visual inspection of the simulations, following the classification scheme by Mellmann.[39] The flow profiles were found to be insensitive to the granular properties, and fully determined by the angular velocity of the drum. Previous studies suggest that the relevant dimensionless number for the flow profile is the Froude number, $\text{Fr} = \Omega^2 R/g$, that is the ratio of centrifugal and gravitational forces.[3,11,57] Hence, we will frequently convert drum angular velocities into Froude numbers for the reader's convenience. The flow profiles in simulations at $\Omega = \pi$ rad/s or 30 revolutions per minute (rpm), corresponding to a Froude number of 0.035, as well as in slower revolving drums, were characterized as being in the rolling regime. A cascading profile was observed in simulations at 2π rad/s or 60 rpm ($\text{Fr} = 0.14$) and 10 rad/s ($\text{Fr} = 0.36$), a cataracting profile for $\Omega = 15$ rad/s ($\text{Fr} = 0.80$) and 16 rad/s ($\text{Fr} = 0.91$), and a cataracting-centrifuging profile for simulations at 18 rad/s ($\text{Fr} = 1.16$) and 19 rad/s ($\text{Fr} = 1.29$). We also verified the existence of a centrifuging profile, in simulations with $\Omega = 25$ rad/s ($\text{Fr} = 2.23$). The simulations at angular velocities between the aforementioned ranges displayed smooth transitions between the flow profiles of the bracketing regimes, hence the aforementioned numbers are not to be interpreted as sharp phase boundaries.

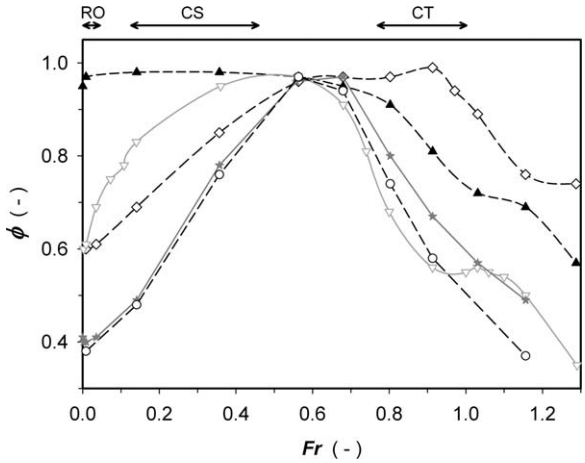

Figure 2. The mixing parameters ϕ of steady-state half-filled drums as functions of the Froude number.

The five bidisperse granular mixtures differ in mass, radius and/or density of the particles. Systems 1 (open triangles), 2 (open diamonds), and 5 (open circles) represent mixtures with identical densities, radii and masses, respectively. System 3 is drawn as solid triangles and System 4 as solid stars, while System 6 is left out as its graph closely follows that of System 5. Further details on the particle properties are provided in Table 2. The arrows at the top of this figure mark the ranges of the rolling (RO), cascading (CS), cataracting (CT), and cataracting-centrifuging (CT/CF) flow regimes.

The rotating drum empowers the four segregation mechanisms, as described in the introduction, to collectively create a mixed or segregated steady state by working in unison or in discord. The final configuration and its degree of mixing, therefore, reflect the relative effectiveness of the four segregation mechanisms within the limitations posed by the flow profile and the particle properties. Figure 2 shows the mixing curves for five systems as a function of angular velocity/Froude number. Each data point represents the average of at least two simulations, including one starting with a randomly filled drum and one initially block-wise segregated drum, typically running for 30 revolutions. From a set of simulations in the flowing regime, differing only in their initial configurations, a standard deviation in the degree of mixing of about 0.03 was established. The mixing curves are remarkably similar for all simulated systems. Segregation predominates at low drum velocities, as illustrated by the snapshots in Figure 3. The degree of mixing ϕ rises with increasing angular velocity, passes through a well-mixed range centered around $\text{Fr} = 0.56$, and then decreases with a further increase in the drum velocity. Movies and snapshots of the simulations confirm this trend of a high degree of mixing at intermediate drum angular velocities, which appears remarkably insensitive to the granular properties, while segregation prevails in both tails of the plot. Inspection of the segregated beds reveals the formation of cylindrical cores running the entire length between the two vertical walls bounding the drum. Interestingly, the radially

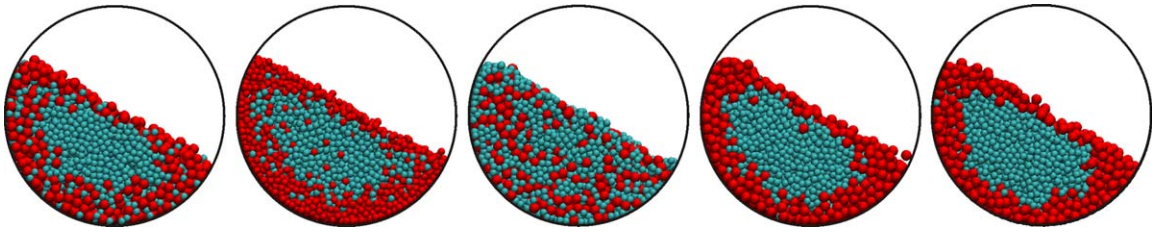

Figure 3. Steady states at low drum angular velocities.

The snapshot show, from left to right, the first five bidisperse beds listed in Table 2, at $\Omega = \pi/2$ rad/s (Fr = 0.035). The *a*-type particles are depicted in light-green, the *b*-type particles in dark red. [Color figure can be viewed in the online issue, which is available at wileyonlinelibrary.com.]

segregated patterns at low Fr are consistently inverted at high Fr. We exploit this property and for clarity henceforth systematically assign the label *a* to the particle type that accumulates in the center at low Fr and in the periphery at high Froude numbers. These simulation results will be discussed below in detail, to analyze which segregation mechanism dominates under specific conditions, where for clarity we have separated the low rotational velocities (flowing and cascading regimes, upto and including optimum mixing) from the high rotational velocities (cataracting and centrifuging regimes, beyond optimum mixing). Note that the simulations of Arntz et al.[48], which include the current reference system, indicate that the peak of optimal mixing shifts with increasing (decreasing) fill levels to higher (lower) rotational velocities.

Low rotational velocities

For low Fr values, well below the mixing maximum, the bed is in the rolling regime. Figures 4 and 5, subfigures A and B, show a densely packed passive bulk that slowly rotates with the drum, with a flowing layer on top.[39,58] The reduced number density, or increased porosity, of this mobile layer is due to the frequent collisions between the relatively fast moving particles under a high local velocity gradient and thereby creates a productive environment for the segregation and mixing mechanisms. With increasing drum velocity, the excited layer grows thicker and less dense, as can be seen from Figures 4 and 5 by comparing sub A and B with sub E and F. Vector plots of the local velocity difference between the two particle types, see the third columns in Figures 4 and 5, indicate where segregation and mixing occur, and thereby permit an interpretation in terms of the four mechanisms. Figures 4C and 5C reveal that in the rolling regime, segregation occurs throughout the flowing layer, while in the mixing regime around Fr = 0.56 the segregation is mainly concentrated in the bottom-right region of the flowing layer, see Figures 4G and 5G. Such a shift of locus is not without consequences, even if the same segregation mechanism remains dominant, for the overall segregation behavior of the bed.[48] Note that subtracting two averages to arrive at a difference one order-of-magnitude smaller is well known to produce a high noise level, unless the two individual averages can be established to a high degree of accuracy. Subdividing the drum into small cells to obtain a spatial distribution reduces the number of particles averaged over and thereby enhances the noise in all plotted distributions. Similar considerations hold true for the noise level in the velocity standard deviations plotted in the fourth columns of Figures 4 and 5, with an accurate standard deviation requiring far more extensive sampling than needed for an accurate average.

The particles in System 1 differ in size and mass, but are of equal density and consequently impervious to the buoyancy mechanism. Our discussion of this system will be brief, because segregation in the absence of buoyancy has been discussed in a number of studies[13,18,40,59] and because a detailed analysis of this particular system has appeared elsewhere.[48] It was argued there that the moderate segregation ($\phi \approx 0.6$) results from the downward percolative motions of the small particles in the flowing layer,[48] culminating in a radial core of the smaller *a*-type granules and a periphery of predominantly the larger *b*-type particles, see Figure 3. The comparison with System 2, to be discussed below, confirms that the mass difference is not responsible for segregation at these low Froude numbers. With increasing angular velocity, that is toward and throughout the cascading regime, the flowing layer becomes more porous, hence less selective to percolation of small particles, and mixing by random collisions gains prominence, as illustrated by Figure 4 of Arntz et al.,[48] achieving a well-mixed state around Fr = 0.56. The latter mixing process is further supported by an increase of the particles' velocities with Fr, which also enhances the inertia mechanism.

The particles in System 2 have distinct densities and masses, but equal radii to eliminate the percolation mechanism. Again, the reduced number density and relatively high velocities of particles in the flowing layer, see Figures 4A, B, E, and F, promote reshuffles of the granules. At low Froude numbers, segregation occurs along the entire length of the flowing layer, see Figure 4C, but most prominently where the layer is at its thickest. The gradual formation of a radial core of the denser *a*-type particles, see Figure 3, is attributed to the buoyancy mechanism, that is the denser particles are sinking down in the flowing layer till they settle on a more closely packed region. Although the *a*- and *b*-type particles are comparable in mass to the *b*- and *a*-type particles of System 1, respectively, the heavier particles accumulate in the core in System 2 but in the periphery in System 1. This indicates that at these low Froude numbers the segregation process is more sensitive to radius and density differences than to mass differences. It then follows that the equal density particles of System 1 segregate by percolation, as was mentioned above, while the equal radius particles of System 2 segregate by buoyancy. With increasing Froude number, the random collision and inertia mechanisms become more important, as illustrated by the large mixing region in Figure 4G, thus reducing and near Fr = 0.56 even suppressing the segregation process in System 2.

In System 3, the radii and densities are chosen such that their associated segregation effects are acting in opposite directions: the percolation mechanism drives the small

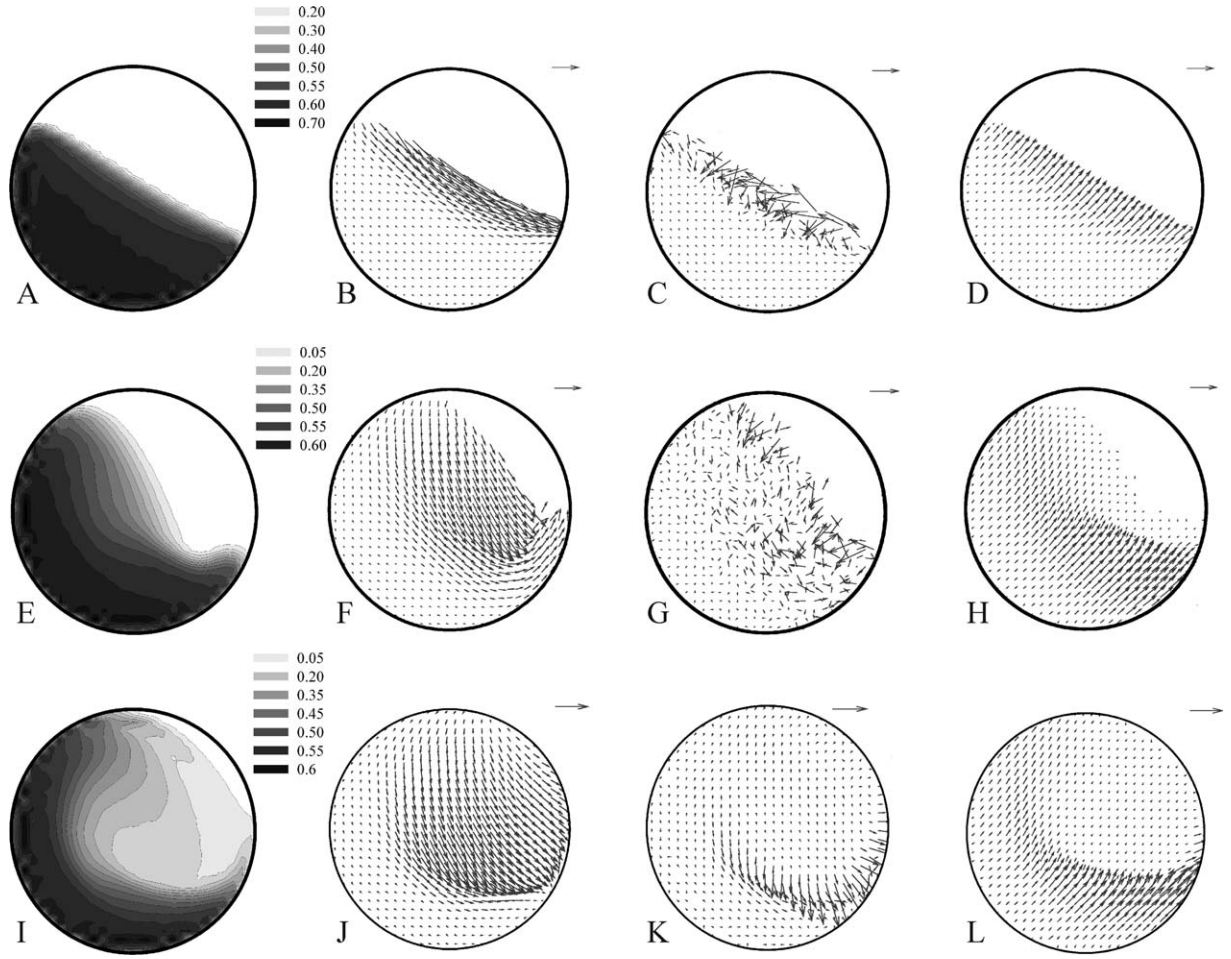

Figure 4. Analysis of the granular bed with particles of equal radius (System 2).

The horizontal rows represent, from top to bottom, beds in the rolling regime ($\Omega = \pi/2$ rad/s, Fr = 0.01), near optimum mixing ($\Omega = 4\pi$ rad/s, Fr = 0.56) and in the cataracting regime ($\Omega = 16$ rad/s, Fr = 0.91). The first vertical column shows the local occupied volume fraction. The second column shows the particle velocities, where we have plotted the relative particle velocity with respect to the uniform rotation of the drum, $\mathbf{v}_i - \boldsymbol{\Omega} \times \mathbf{r}_i$, rather than the absolute velocity, for clarity of the plot and for easy identification of the active region(s). The reference arrows in the top right corners represent 0.2, 0.9, and 1.1 m/s, respectively, from top to bottom. The third column illustrates the velocity difference between the two particle types, $\mathbf{v}_a - \mathbf{v}_b$, with reference arrows of 0.013, 0.05, and 0.14 m/s, respectively. The fourth column shows the width of the local velocity distribution, where the horizontal (vertical) components of the plotted vectors denote the standard deviations along the horizontal (vertical) direction, with reference arrows measuring 0.013, 0.03, and 0.05 m/s, respectively.

particles (of low density) to the radial core, whereas the buoyancy mechanism strives for a core of the high-density particles (of large radius). Figures 2 and 3 show that this system remains well-mixed for angular drum velocities in the rolling and cascading regimes.[12,19,24] The absence of segregation, despite the order-of-magnitude difference in the particles's masses, provides further support for the aforementioned observation that inertia is of little importance at these low Froude numbers.

If, in contrast, the particles of one type are both smaller and denser than the particles of the other type, as in Systems4, 5 and 6, then buoyancy and percolation co-operate in driving the smaller and denser *a*-type particles to the radial core, see Figure 3. The mixing parameter, see Figure 2, indicates that the resulting segregation is indeed more intense than in Systems 1 and 2, as is also clear from Figure 3, where only either one of these two mechanisms is active. Here again, the segregation becomes less intense and eventually vanishes with the Froude number rising to 0.56. A comparison of Systems 4 and 6 shows that an increase in the density ratio, from 3 to 4, does not significantly enhance segregation, suggesting that the buoyancy mechanism has already reached its optimal performance at the former ratio.

High rotational velocities

At high angular velocities beyond the optimum mixing regime, that is for Froude numbers exceeding 0.56, the bed is in the cataracting, cataracting-centrifuging, or centrifuging regime. For the cataracting regime, Figures 4 and 5, subfigures I and J show that particles with high mobilities are thinly distributed over a large volume of the box, thus offering a high potential for intermixing. The plots in the second row of Figure 6, however, indicate that the particles following ballistic trajectories through the sparsely populated volume above the bed collide only infrequently and hence hardly contribute to (de)mixing. The particles rolling down the diffuse surface of the bed, see Figures 4J and 5J, are susceptible to segregation by percolation and buoyancy, as visible in the second row of Figure 6. Both particle flows are

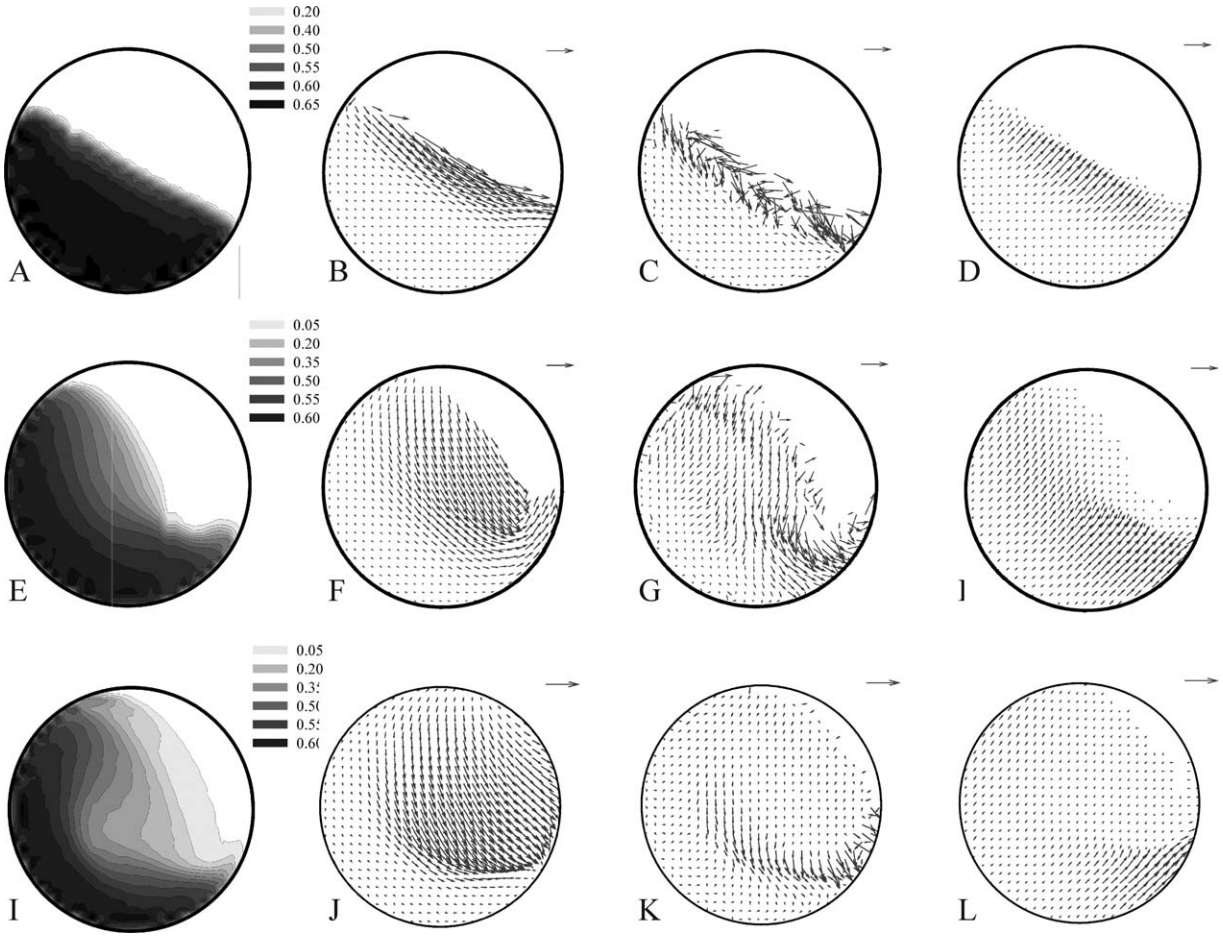

Figure 5. Analysis of the granular bed with particles of nearly equal mass (System 4).

The conditions and set-ups of the subgraphs are identical to those used in Figure 4. Note the strong similarities with System 2, see Figure 4, despite the marked differences in the radius and mass of the *b*-type particles in Systems 2 and 4 (the *a*-type particles are identical). The deviations are largely limited to the velocity differences and velocity standard deviations at the higher Froude numbers.

reunited at the lower end of the flowing layer, which appears in the second row of Figure 6 as the dominant region of segregation. In the cataracting-centrifuging and centrifuging regimes, that is for Froude numbers above 1.0, one or more layers of centrifuging particles cover the entire drum well. These layers may show buoyancy and percolation effects, with the denser or smaller particles moving radially outward, respectively. At higher drum velocities, the bed becomes too closely packed to permit relative particle motions, and airborne particles impinging on the inner centrifuging layer make a small contribution to the (de)mixing process.

The reference system, with particles bidisperse in size and mass, shows a moderate to intense segregation at high Froude numbers. At equal particle densities, this segregation most likely results from percolation in the flowing layer, as is further supported by the observations for the other systems to be discussed below. Arntz et al. [48] argued that the shift of the main percolation region from the center of the flowing layer in the flowing regime to the tail of the flowing layer in the cataracting regime is responsible for inverting the net effect of the percolation mechanism, which thus for Froude numbers approaching unity gives rise to a radial core of large particles ("inverse radial segregation", see the snapshots in the first column of Figure 6) while a radial core of small particles forms at low Fr (regular radial segregation, see Figure 3). The mixing parameter of System 1 shows a short plateau for Froude numbers from 0.9 to 1.1, and smaller fluctuations are visible for the other systems near the same range of Froude numbers. As this plateau is unexpected, we performed supplementary simulations, both at the originally selected angular velocities and at additional intermediate values (see Figure 2), which confirm that the shoulder reproduces. Most likely, this plateau reflects that the bed is still slowly evolving when the simulations were discontinued after 30 revolutions. A selected number of simulations were continued for many more revolutions, but this hardly changed the degrees of mixing in these drums, indicating that the final steady state is being approached only very slowly. This slight indeterminacy in the steady-state degree of mixing does, of course, not alter the main observation that the particles tend to segregate at high drum velocities.

The equal radius particles of System 2 are well mixed in the cataracting regime, thereby suggesting that a mass or density difference is insufficient to induce segregation in this Froude regime and confirming that percolation is the driving mechanism for System 1 in the cataracting regime. The velocity difference plots in the second column of Figure 6 show outward pointing arrows at the lower right side, indicative of inward motion of the lighter *b*-type particles relative

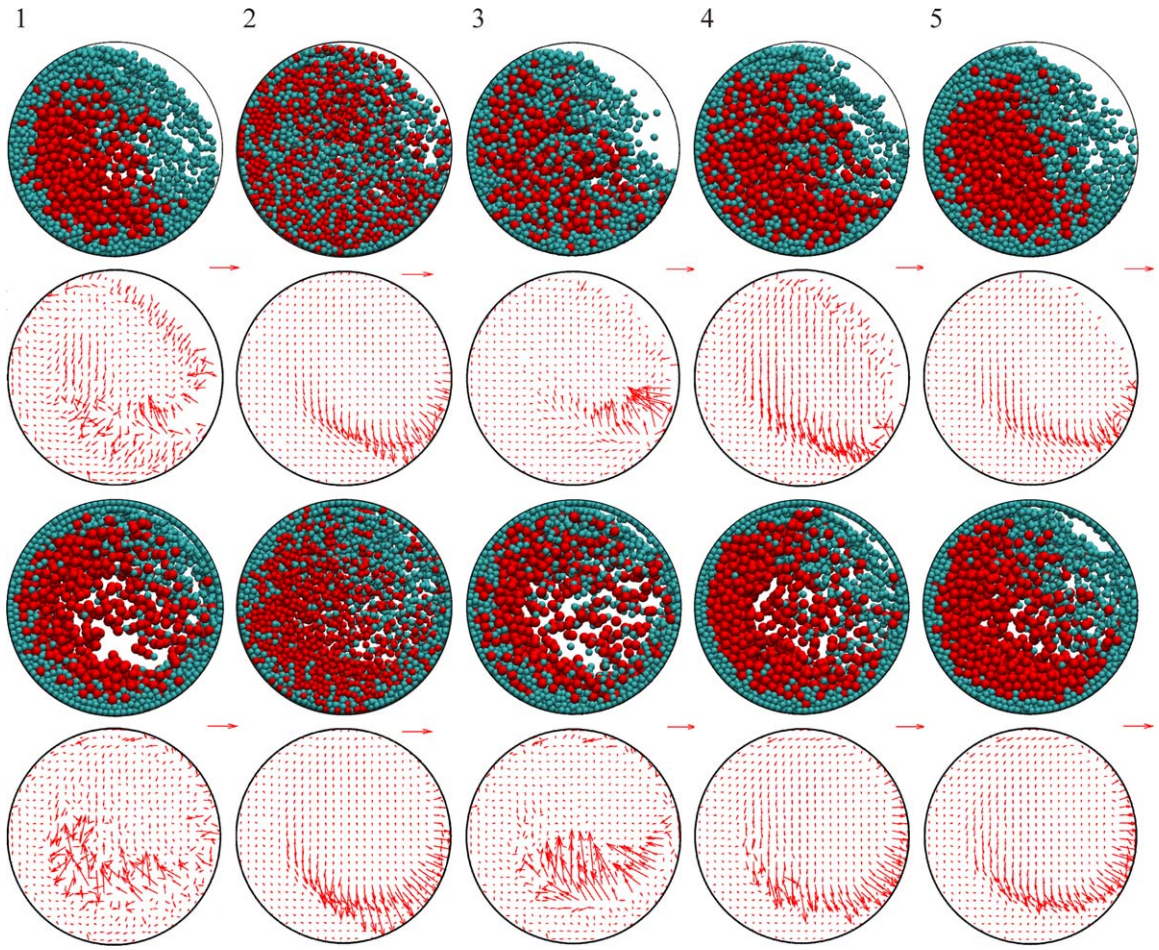

Figure 6. Snapshots and velocity-difference plots at high drum angular velocities.

Shown are Systems 1–5 (from left to right) at drum angular velocities of 16 rad/s (Fr = 0.91, cataracting) in the top two rows and at 18 rad/s (Fr = 1.16, cataracting-centrifuging) in the bottom two rows. The *a*-type particles are depicted in light-green, the *b*-type particles in dark red. The reference arrows in the second row correspond with 0.04, 0.14, 0.10, 0.10, and 0.14 m/s, and those in the fourth row with 0.08, 0.17, 0.07, 0.20, and 0.22 m/s. [Color figure can be viewed in the online issue, which is available at wileyonlinelibrary.com.]

to the denser and heavier *a*-type particles. A more detailed analysis and visual inspection of movies reveal that in this region the airborne particles impinge on the bed surface, often bouncing back before being taken up by the bed. The inertia mechanism, that is lighter particles rebound more strongly than heavier particles, then gives rise to the velocity differences, see the second column of Figure 6, and large standard deviations, see Figure 4L, in this region. The random nature of the collisions, with light and heavy particles bouncing back in various directions, appears to promote mixing and effectively suppresses possible segregation mechanisms. A gradual decrease of the order parameter is observed for Froude numbers exceeding 0.9, where the buoyancy effect induced by the centrifugal pseudo force drives the denser *a*-type particles to the drum wall (recall that the particles in System 2 are of equal size, thereby eliminating the percolation mechanism).

The properties of the particles in System 3—small low-density particles and large high-density particles—were specifically chosen to balance the percolation and buoyancy mechanisms in the rolling and cascading regimes. Figure 2 and the third column of Figure 6 show that this balance does not extend to the cataracting and centrifuging regimes. The accumulation of the small low-density particles at the drum wall, be it with a higher degree of mixing than in System 1, indicates that percolation has gained the upper hand over buoyancy.

The radius and density combination in System 4 yields two particle types with comparable masses and thus largely eliminates the inertia mechanism. The standard deviations in the velocities are considerably reduced relative to those of the unequal mass particles in System 2, as can be seen by comparing Figure 5L with Figure 4L. The percolation and buoyancy mechanisms are seen to collaborate in driving the denser and smaller *a*-type particle to the periphery, see the fourth column in Figure 6. A similar cooperative effect dominates in System 5, whose particles of exactly equal mass are seen to segregate in the fifth column of Figure 6, and in System 6, where the smaller particles are heavier than the larger particles.

Other particle properties

Besides the radius, mass, and density, we have also systematically varied all other particle parameters appearing in the force Eqs. 1–3 and assessed their respective influences on the segregation process. These simulations were mainly carried out using the reference system, setting all parameters to the default values listed in the second column of Table 1.

The properties of all *a*-type or all *b*-type particles were altered, one by one, over the ranges indicated in the third column of Table 1. Most simulations were confined to the rolling regime, to keep the required computer time manageable, with brief excursions to other systems and higher drum angular velocities to confirm the general validity of our findings. While changes in the radius (System 2) or density (Systems 3–6) relative to the reference system notably affect the degree of mixing, the explored variations of the dynamic interparticle friction coefficients between *a*-type particles μ^t_{aa}, between *b*-type particles μ^t_{bb}, and between mixed particle pairs μ^t_{ab}, the particle–wall friction coefficients μ^t_{pw}, with $p = a$ or $p = b$, the particle–particle and particle–wall tangential damping coefficients η^t_{pp} and η^t_{pw}, the particle–particle elastic stiffness k^n_{pp} and the normal damping coefficients η^n_{pp} and η^n_{pw} (which are related to the tabulated restitution coefficients e^n_{pp} and e^n_{pw}) hardly affect the mixing behavior. Only at certain extreme values are differences detectable, like a bed that remains immobile at very low particle–wall friction coefficients or an increased degree of mixing for fully elastic $\left(e^n_{pp}=1\right)$ particle–particle collisions.

Of particular interest is the roughness of the particles, which is represented in the current simulation model by the dynamic friction coefficient μ^t_{pp} and the damping coefficient η^t_{pp}, because some simulation models are built on the assumption that differences in roughness give rise to segregation.[1,60] We find no evidence for this assumption in the reference system, in line with the experimental observations by Pohlman et al.[61] Only at low friction coefficients, that is for μ^t_{pp} below about 0.25, are there noticeable deviations. In mixtures of rough and very smooth particles, we observe that a thin layer of predominantly smooth particles forms at the vertical drum walls while the middle of the drum remains similar to that in the reference simulation. Furthermore, mixtures of smooth particles appear to segregate less well, with more small particles at the periphery and more large particles in the core, than otherwise equal mixtures of rough particles.

Conclusions

The mixing and segregation behavior of bidisperse granular beds in horizontal rotating drums will, at least in principle, depend on all mechanical properties of the granular particles involved. We have performed an extensive set of DEM simulations to assess the impact of a dozen properties and find that three parameters dominate the (de)mixing behavior, namely the differences in radii, densities, and masses of the two particle types in the drum. These three parameters are related to the percolation, buoyancy, and inertia mechanisms, respectively, which in a rotating drum compete with the ubiquitous random collisions to establish a steady state. For the six systems studied here, percolation emerges as the dominant mechanism driving segregation. Percolation is observed to be active in the rolling and cascading regime, collecting the smaller particles in a central core, as well as in the cataracting and centrifuging regimes, driving the smaller particles to the cylindrical drum wall. Only for angular drum velocities intermediate between the cascading and cataracting regime does the granular bed mix. This increase and subsequent decrease of the degree of mixing with increasing drum angular velocity, see Figure 2, is in agreement with the trend observed in experiments.[40] A remarkable pivotal point is reached at a Froude number of 0.56, where all simulated systems attain a well-mixed steady state. The picture that emerges in this study, building on the earlier ideas by Nityanand et al.[40] and Arntz et al.[48], is that the relative efficiencies of the four segregation and mixing mechanisms, and hence the degree of segregation in the stationary state, are largely determined by the prevailing flow regime. The latter, in turn, is controlled and established by the angular velocity of the drum (and the fill level of the drum[48]) and appears insensitive to the radii, densities, and masses of the particles. Other particle properties, like their elasticity and the friction coefficients for normal and tangential motion, appear to be of minor consequence for the segregation process.

Acknowledgments

The project was financially supported through a grant from the Program Economy, Ecology, and Technology (E.E.T.) by The Netherlands' Department of Economic Affairs, the Department of Public Housing, Spatial Planning, and Environmental Protection, and the Department of Education, Cultural Affairs, and Sciences.

Literature Cited

1. Chakraborty S, Nott PR, Prakash JR. Analysis of radial segregation of granular mixtures in a rotating drum. *Eur Phys J E*. 2000;1(4):265–273.
2. Rapaport DC. Radial and axial segregation of granular matter in a rotating cylinder: A simulation study. *Phys Rev E*. 2007;75(3):031301.
3. Turner JL, Nakagawa M. Particle mixing in a nearly filled horizontal cylinder through phase inversion. *Powder Technol*. 2000;113(1–2):119–123.
4. Khakhar DV, Orpe AV, Hajra SK. Segregation of granular materials in rotating cylinders. *Physica A*. 2003;318(1–2):129–136.
5. Di Renzo A, Di Maio FP. Comparison of contact-force models for the simulation of collisions in DEM-based granular flow codes. *Chem Eng Sci*. 2004;59(3):525–541.
6. Aranson IS, Tsimring LS. Patterns and collective behavior in granular media: Theoretical concepts. *Rev Mod Phys*. 2006;78(2):641–692.
7. Bridgwater J. Mixing of powders and granular materials by mechanical means-A perspective. *Particuology* 2012;10(4):397–427.
8. Duran J. Sand, Powders and Grains: An Introduction to the Physics of Granular Materials. New York: Springer, 2000.
9. Seiden G, Thomas PJ. Complexity, segregation, and pattern formation in rotating-drum flows. *Rev Mod Phys*. 2011;83(4):1323–1365.
10. Zhu HP, Zhou ZY, Yang RY, Yu AB. Discrete particle simulation of particulate systems: a review of major applications and findings. *Chem Eng Sci*. 2008;63(23):5728–5770.
11. Ottino JM, Khakhar DV. Mixing and segregation of granular materials. *Annu Rev Fluid Mech*. 2000;32:55–91.
12. Jain N, Ottino JM, Lueptow RM. Combined size and density segregation and mixing in noncircular tumblers. *Phys Rev E*. 2005;71(5):051301.
13. Dury CM, Ristow GH. Radial segregation in a two-dimensional rotating drum. *J Phys I*. 1997;7(5):737–745.
14. Thomas N. Reverse and intermediate segregation of large beads in dry granular media. *Phys Rev E*. 2000;62(1):961–974.
15. Ding YL, Forster R, Seville JPK, Parker DJ. Segregation of granular flow in the transverse plane of a rolling mode rotating drum. *Int J Multiphase Flow*. 2002;28(4):635–663.
16. Hajra SK, Khakhar DV. Sensitivity of granular segregation of mixtures in quasi-two-dimensional fluidized layers. *Phys Rev E*. 2004;69(3):031304.
17. Kawaguchi T, Tsutsumi K, Tsuji Y. MRI measurement of granular motion in a rotating drum. *Part Part Syst Charact*. 2006;23(3–4):266–271.
18. Savage SB, Lun CKK. Particle-size segregation in inclined chute flow of dry cohesionless granular solids. *J Fluid Mech*. 1988;189:311–335.

19. Jain N, Ottino JM, Lueptow RM. Regimes of segregation and mixing in combined size and density granular systems: an experimental study. *Granular Matter*. 2005;7(2-3):69–81.
20. Khakhar DV, Orpe AV, Ottino JM. Continuum model of mixing and size segregation in a rotating cylinder: concentration-flow coupling and streak formation. *Powder Technol*. 2001;116(2–3):232–245.
21. Metcalfe G, Graham L, Zhou J, Liffman K. Measurement of particle motions within tumbling granular flows. *Chaos*. 1999;9(3):581–593.
22. Pereira GG, Sinnott MD, Cleary PW, Liffman K, Metcalfe G, Sutalo ID. Insights from simulations into mechanisms for density segregation of granular mixtures in rotating cylinders. *Granular Matter*. 2011;13(1):53–74.
23. Ristow GH. Particle mass segregation in a 2-dimensional rotating drum. *Europhys Lett*. 1994;28(2):97–101.
24. Alonso M, Satoh M, Miyanami K. Optimum combination of size ratio, density ratio and concentration to minimize free-surface segregation. *Powder Technol*. 1991;68(2):145–152.
25. Felix G, Thomas N. Evidence of two effects in the size segregation process in dry granular media. *Phys Rev E*. 2004;70(5):051307.
26. Alizadeh E, Dubé O, Bertrand F, Chaouki J. Characterization of mixing and size segregation in a rotating drum by a particle tracking method. *AIChE J*. 2013;59(6):1894–1905.
27. Chen PF, Ottino JM, Lueptow RM. Subsurface granular flow in rotating tumblers: a detailed computational study. *Phys Rev E*. 2008; 78(2):021303.
28. Huang AN, Kuo HP. A study of the three-dimensional particle size segregation structure in a rotating drum. *AIChE J*. 2012;58(4):1076–1083.
29. Kuo HP, Hsu RC, Hsiao YC. Investigation of axial segregation in a rotating drum. *Powder Technol*. 2005;153(3):196–203.
30. Rapaport DC. Radial and axial segregation of granular matter in a rotating cylinder: A simulation study. *Phys Rev E*. 2007;75(3): 031301.
31. Arntz MMHD, den Otter WK, Beeftink HH, Boom RM, Briels WJ. Repeated segregation and energy dissipation in an axially segregated granular bed. *Europhys Lett*. 2010;92:54004.
32. Chen P, Ottino JM, Lueptow RM. Onset mechanism for granular axial band formation in rotating tumblers. *Phys Rev Lett*. *7* 2010; 104(18):188002.
33. Lee C-F, Chou H-T, Capart H. Granular segregation in narrow rotational drums with different wall roughness: symmetrical and asymmetrical patterns. *Powder Technol*. 2013;233:103–115.
34. Alizadeh E, Dubé O, Bertrand F, Chaouki J. Characterization of mixing and size segregation in a rotating drum by a particle tracking method. *AIChE J*. 2013;59(6):1894–1905.
35. Arntz MMHD, den Otter WK, Beeftink HH, Boom RM, Briels WJ. The influence of end walls on the segregation pattern in a horizontal rotating drum. *Granular Matter*. 2013;15(1):25–38.
36. Santomaso AC, Ding YL, Lickiss JR, York DW. Investigation of the granular behaviour in a rotating drum operated over a wide range of rotational speed. *Chem Eng Res Des*. 2003;81(A8):936–945.
37. Yang RY, Yu AB, McElroy L, Bao J. Numerical simulation of particle dynamics in different flow regimes in a rotating drum. *Powder Technol*. 2008;188(2):170–177.
38. Henein H, Brimacombe JK, Watkinson AP. Experimental-study of transverse bed motion in rotary kilns. *Metall Trans B–Process Metall*. 1983;14(2):191–205.
39. Mellmann J. The transverse motion of solids in rotating cylinders - forms of motion and transition behavior. *Powder Technol*. 2001; 118(3):251–270.
40. Nityanand N, Manley B, Henein H. An analysis of radial segregation for different sized spherical solids in rotary cylinders. *Metall Trans B–Process Metall*. 1986;17(2):247–257.
41. Pöschel T, Schwager T. Computational Granular Dynamics: Models and Algorithms: Berlin: Springer, 2005.
42. Zhu HP, Zhou ZY, Yang RY, Yu AB. Discrete particle simulation of particulate systems: theoretical developments. *Chem Eng Sci*. 2007;62(13):3378–3396.
43. Thompson PA, Grest GS. Granular flow – friction and the dilatancy transition. *Phys Rev Lett*. 1991;67(13):1751–1754.
44. Khakhar DV, McCarthy JJ, Ottino JM. Radial segregation of granular mixtures in rotating cylinders. *Phys Fluids*. 1997;9(12):3600–3614.
45. Poschel T, Herrmann HJ. Size segregation and convection. *Europhys Lett*. 1995;29(2):123–128.
46. Cundall PA, Strack ODL. Discrete numerical-model for granular assemblies. *Geotechnique* 1979;29(1):47–65.
47. Hoomans BPB. Granulas Dynamics of Gas-Solid Two-Phase Flows, PhD thesis. Enschede, University of Twente, 2000.
48. Arntz MMHD, den Otter WK, Briels WJ, Bussmann PJT, Beeftink HH, Boom RM. Granular mixing and segregation in a horizontal rotating drum: a simulation study on the impact of rotational speed and fill level. *AIChE J*. 2008;54(12):3133–3146.
49. Schäfer J, Dippel S, Wolf DE. Force schemes in simulations of granular materials. *J Phys I*. 1996;6(1):5–20.
50. Allen MP, Tildesley DJ. Computer Simulations of Liquids. Oxford: Oxford University Press, 1993.
51. Cleary PW, Metcalfe G, Liffman K. How well do discrete element granular flow models capture the essentials of mixing processes? *Appl Math Model*. 1998;22(12):995–1008.
52. Dury CM, Ristow GH. Competition of mixing and segregation in rotating cylinders. *Phys Fluids*. 1999;11(6):1387–1394.
53. Porion P, Sommier N, Faugere AM, Evesque P. Dynamics of size segregation and mixing of granular materials in a 3D-blender by NMR imaging investigation. *Powder Technol*. 2004;141(1-2):55–68.
54. Van Puyvelde DR. Simulating the mixing and segregation of solids in the transverse section of a rotating kiln. *Powder Technol*. 2006; 164(1):1–12.
55. Humphrey W, Dalke A, Schulten K. VMD: Visual molecular dynamics. *J Mol Graph* 1996;14(1):33–38.
56. McCarthy JJ, Ottino JM. Particle dynamics simulation: a hybrid technique applied to granular mixing. *Powder Technol*. 1998;97(2): 91–99.
57. Arntz MMHD, den Otter WK, Beeftink HH, Bussmann PJT, Briels WJ, Boom RM. Granular mixing and segregation in a horizontal rotating drum: a simulation study on the impact of rotational speed and fill level. *AIChE J*. 2008;54(12):3133–3146.
58. Nakagawa M, Altobelli SA, Caprihan A, Fukushima E, Jeong EK. Noninvasive measurements of granular flows by magnetic-resonance-imaging. *Exp Fluids*. 1993;16(1):54–60.
59. Cantelaube F, Bideau D. Radial Segregation in a 2d Drum – an experimental-analysis. *Europhys Lett*. 1995;30(3):133–138.
60. Puri S, Hayakawa H. Segregation of granular mixtures in a rotating drum. *Physica A*. 2001;290(1–2):218–242.
61. Pohlman NA, Ottino JM, Lueptow RM. End-wall effects in granular tumblers: from quasi-two-dimensional flow to three-dimensional flow. *Phys Rev E*. 2006;74(3):031305.

Manuscript received Sept. 12, 2012, revision received Jun. 12, 2013, and final revision received Sept. 16, 2013.